Disruption of mouse *ERCC1* results in a novel repair syndrome with growth failure, nuclear abnormalities and senescence

G. Weeda*, I. Donker*, J. de Wit*, H. Morreau†, R. Janssens*, C.J. Vissers‡, A. Nigg‡, H. van Steeg§, D. Bootsma* and J.H.J. Hoeijmakers*

Background: The structure-specific ERCC1/XPF endonuclease complex that contains the ERCC1 and XPF subunits is implicated in the repair of two distinct types of lesions in DNA: nucleotide excision repair (NER) for ultraviolet-induced lesions and bulky chemical adducts; and recombination repair of the very genotoxic interstrand cross-links.

Results: Here, we present a detailed analysis of two types of mice with mutations in *ERCC1*, one in which the gene is 'knocked out', and one in which the encoded protein contains a seven amino-acid carboxy-terminal truncation. In addition to the previously reported symptoms of severe runting, abnormalities of liver nuclei and greatly reduced lifespan (which appeared less severe in the truncation mutant), both types of *ERCC1*-mutant mouse exhibited an absence of subcutaneous fat, early onset of ferritin deposition in the spleen, kidney malfunction, gross abnormalities of ploidy and cytoplasmic invaginations in nuclei of liver and kidney, and compromised NER and cross-link repair. We also found that heterozygosity for *ERCC1* mutations did not appear to provide a selective advantage for chemically induced tumorigenesis. An important clue to the cause of the very severe *ERCC1*-mutant phenotypes is our finding that *ERCC1*-mutant cells undergo premature replicative senescence, unlike cells from mice with a defect only in NER.

Conclusions: Our results strongly suggest that the accumulation in *ERCC1*-mutant mice of endogenously generated DNA interstrand cross-links, which are normally repaired by ERCC1-dependent recombination repair, underlies both the early onset of cell cycle arrest and polyploidy in the liver and kidney. Thus, our work provides an insight into the molecular basis of ageing and highlights the role of ERCC1 and interstrand DNA cross-links.

Addresses: *Department of Cell Biology and Genetics, Medical Genetics Center, Erasmus University, Rotterdam P.O. Box 1738, 3000 DR Rotterdam, The Netherlands. †Department of Pathology, Leiden University Hospital, Leiden P.O. Box 9600, 2300 RC Leiden, The Netherlands. ‡Department of Pathology, Erasmus University, 3000 DR Rotterdam, The Netherlands. §Laboratory of Health Effects Research, National Institute of Public Health and the Environment, P.O. Box 1, 3720 BA Bilthoven, The Netherlands.

Correspondence: J.H.J. Hoeijmakers
E-mail: hoeijmakers@gen.fgg.eur.nl

Received: **14 March 1997**
Revised: **21 April 1997**
Accepted: **21 April 1997**

Published: **21 May 1997**

Current Biology 1997, 7:427–439
http://biomednet.com/elecref/0960982200700427

Background

The nucleotide excision repair (NER) process recognizes and eliminates a very broad spectrum of structurally diverse DNA lesions [1]. The consequences of inborn defects in NER are apparent from the rare human autosomal recessive syndrome xeroderma pigmentosum (XP), characterized by ultraviolet light (UV) sensitivity to the sun, pigmentation abnormalities, strong predisposition to skin cancer in exposed areas, and frequently accelerated neurodegeneration. Two other distinct NER disorders have been recognized in humans: the severe neurodevelopmental conditions Cockayne syndrome (CS) and trichothiodystrophy (TTD) (for a review see [2] and references therein). In remarkable contrast to XP, neither CS nor TTD is apparently associated with a clear predisposition to skin cancer. These three NER syndromes are genetically heterogeneous and comprise at least ten complementation groups: seven in XP (XP-A to XP-G), two in CS (CS-A and CS-B) and three in TTD (TTD-A, and two that are simultaneously XP groups: XP-B and XP-D) [3].

In addition to the human NER disorders, there is a second type of mammalian NER mutant: UV-sensitive rodent cell lines (complementation groups 1–11, which can be corrected by human *ERCC* genes). The *ERCC1* gene corrects the repair defects of group 1 mutants, which are (like other NER mutants) sensitive to UV, but which alone with group 4 mutants are additionally very sensitive to DNA cross-linking agents [4]. *ERCC1* is not implicated in any of the known XP, CS or TTD complementation groups [5].

The NER process entails damage recognition followed by a 'cut-and-paste' mechanism involving a large number of proteins [3,6]. The *ERCC1* product was recently found to reside with the XPF protein (also known as ERCC4) in a complex which constitutes a structure-specific endonuclease responsible for the incision in the damaged strand 5′ of the lesion [7,8]. The first 214 amino acids of the ERCC1 protein are significantly homologous to the yeast NER factor RAD10 [9], which is complexed with RAD1, the yeast homologue of XPF [10,11]. Importantly, both yeast

homologues are involved in two processes: NER and a mitotic recombination pathway [12]. This explains the sensitivity of *ERCC1* and *ERCC4* mutants to DNA cross-links, which require mitotic recombination for their repair. The remaining carboxy-terminal 80 amino acids of ERCC1, which are not similar to RAD10, share clear homology with the carboxyl terminus of the *Escherichia coli* NER endonuclease UvrC [13], and are also similar to numerous other nucleases [14]. Consistent with an anticipated nuclease-related function of this domain, our previous mutational analysis of ERCC1 has revealed that deletion of the last four amino acids mildly affects NER and cross-link repair, but that truncation of five or six residues severely impairs both repair functions [14]. In contrast, deletion of the less conserved first 91 residues has no significant effect on its function.

A severe *ERCC1* mouse mutant, which displayed disturbed growth, reduced life span and abnormalities of liver nuclei, was described previously by McWhir and collaborators [15]. In our study, we have generated two types of mouse mutated at *ERCC1*: one in which the gene is 'knocked out' and one in which it is partially inactivated by introducing, into the encoded protein, a carboxy-terminal truncation that starts immediately after the carboxy-terminal UvrC-homologous region. We have previously shown that this seven amino-acid truncation includes two amino acids of the domain found to be important for ERCC1 function as determined *in vitro*, but does not cause dramatic protein instability [14]. In addition to the features of *ERCC1*-mutant mice described by McWhir and coworkers [15], we provide evidence for spleen, kidney and cutaneous deficits, and also a detailed analysis of NER, cross-link repair, cell cycle arrest and replicative senescence. Importantly, our results suggest that the accumulation of endogenous cross-links as a result of *ERCC1* inactivation leads to genomic instability and significantly contributes to ageing in mice.

Results

Targeting of the *ERCC1* gene in embryonic stem cells

The minimal size of the functional ERCC1 protein that we have previously deduced from *in vitro* deletion analysis [14] is depicted schematically in Figure 1a. The targeting constructs used for knockout and partial inactivation of the gene and the various probes used for screening and verification of the homologous recombination are outlined in Figures 1b and 2b. The knockout vector consisted of an approximately 9.5 kb isogenic mouse genomic *Hin*dIII/*Sal*I DNA fragment, in which a pMC1–*neo* cassette [16] interrupts exon 7, thus aborting the essential carboxy-terminal 74 amino acids (Fig. 1b).

The design of a construct for a more subtle mutation, truncating the protein close to the end of the essential region, was complicated. The human and mouse *ERCC1* loci contain another gene of unknown function which overlaps the last exon of *ERCC1* in the antisense direction ([17] and data not shown). In order to avoid interference with this function, we inserted the *neo* marker into the last intron of *ERCC1*. This strategy gave the additional advantage that *ERCC1* transcription and mRNA processing would remain intact and that the *neo* resistance gene would be removed by splicing. The replacement-type vector also introduced a premature stop codon at position 292 of mouse ERCC1, removing the last seven amino acids (note that the mouse ERCC1 protein has one residue more than human ERCC1). Thus, the encoded protein (ERCC1^{*292}) terminates immediately after the UvrC-homologous region (Figs 1a,2a). Our previously reported *ERCC1* mutational analysis indicated, however, that the truncation removes just two amino acids of the ERCC1 essential domain, but should not dramatically decrease protein stability [14].

Targeting of both constructs was evaluated by Southern blot analysis using unique probes that hybridize outside the targeting constructs (Figs 1c,2c). The frequency of homologous recombination for the knockout and *ERCC1*^{*292} constructs was approximately 5% (8 of 170 G418-resistant transformants) and 13% (23 of the 172 clones analyzed), respectively. In the case of the *ERCC1*^{*292} mutation, two of the independent embryonic stem (ES) cell clones were also analyzed by reverse-transcriptase-coupled polymerase chain reaction (RT-PCR), using *ERCC1*-specific cDNA primers and DNA sequencing to verify the presence of the mutation and to ensure that the rest of the coding region, which was part of the targeting construct, was still intact after the process of homologous recombination.

Generation of *ERCC1*-mutant mice and analysis of *ERCC1* expression

F2 offspring from each of two independent *ERCC1* knockout and *ERCC1*^{*292} ES cell clones were born, and expression of the targeted gene was analyzed at the mRNA level in mouse embryonic fibroblasts (MEFs), using RT-PCR and dot-blot analysis (Fig. 3). Filters were hybridized with wild-type or mutant-specific ^{32}P-labelled oligonucleotides, which distinguished *ERCC1*^{*292} transcripts from wild-type. PCR products from fibroblasts of F2 offspring of the *ERCC1*-knockout ES cell clones hybridized only to the wild-type-specific primer if the offspring were wild-type homozygous or heterozygous, whereas no mRNA could be detected in homozygous mutant MEFs. RNA from heterozygous *ERCC1*^{*292} MEFs clearly hybridized to both probes; in homozygous mutant *ERCC1*^{*292} MEFs, only mutant transcript could be detected. We conclude that the knockout allele is transcriptionally inactivated and that the *ERCC1*^{*292} allele is still transcribed and, as shown by sequence analysis (data not shown), is properly processed.

In order to determine the relative levels of *ERCC1*^{*292} message more accurately, RT-PCR products (from

Figure 1

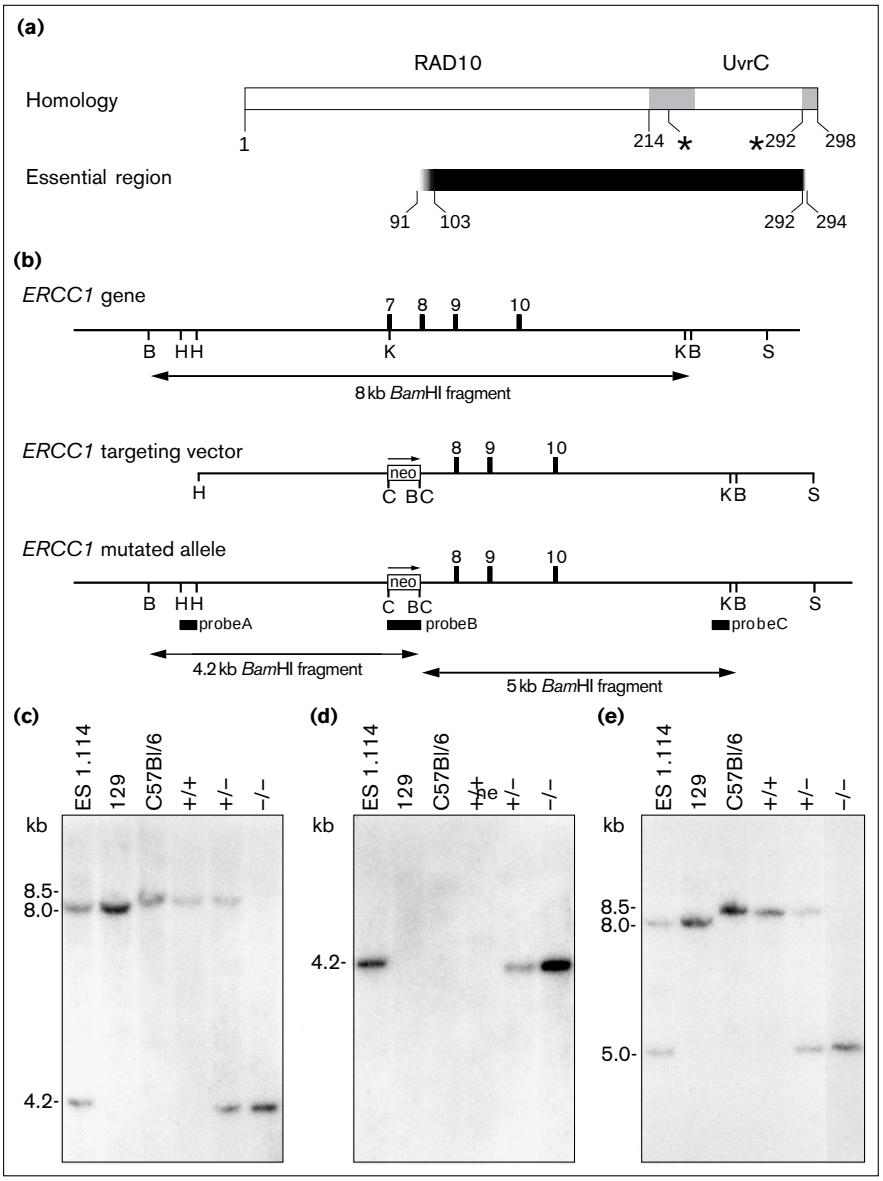

Disruption of the *ERCC1* gene: the knockout construct. **(a)** The mouse ERCC1 protein, showing regions homologous to yeast RAD10 and *E. coli* UvrC (in white), the minimal functional region (in black), and the positions of the neomycin insertion in the knockout (*) and of the subtle mutation in the partial inactivation mutant (*292). **(b)** Strategy for inactivation of the *ERCC1* gene by homologous recombination in embryonic stem (ES) cells. Part of the genomic structure of the wild-type and mutated *ERCC1* gene is depicted, showing *Bam*HI (B), *Cla*I (C), *Hin*dIII (H), *Kpn*I (K), and *Sal*I (S) restriction sites. Exons are numbered and indicated by black bars above the line. Black boxes below the line denote the DNA probes A, B and C used for Southern blot analysis. The *neo* cassette containing a diagnostic *Bam*HI restriction site was inserted into a *Cla*I site that was generated by site-directed mutagenesis in exon 7; the small arrows mark the direction of *neo* transcription. Probe A detects a 4.2 kb and an 8 or 8.5 kb *Bam*HI fragment (due to polymorphic differences between 129 and C57Bl/6 DNA) in the mutant and wild-type alleles, respectively. Probe B covers the coding region of the dominant selectable marker *neo*. Probe C hybridizes to a 5 kb and an 8 or 8.5 kb *Bam*HI fragment in the mutant and wild-type alleles, respectively. **(c–e)** Southern blot analysis of *Bam*HI-digested genomic DNA from an ES cell clone (ES 1.14) and tail DNA from litter-mates – homozygous wild-type (+/+), heterozygous (+/–) and homozygous mutant (–/–) – from an intercross of mice heterozygous for *ERCC1* knockout. As a control, DNA from strains 129 and C57Bl/6 was included. Homologous recombination was indicated by (c) probe A hybridizing to a 4.2 kb fragment, (d) probe B hybridizing to a 4.2 kb fragment and (e) probe C hybridizing to a 5 kb fragment.

ERCC1^{*292} ES cells) were subcloned. Dot-blot analysis revealed that, in 9 out of 70 recombinant clones, the desired mutation could be detected (data not shown), indicating that the transcript level from the *ERCC1*^{*292} allele is reduced to about 15% of the level of the non-targeted allele. In an attempt to confirm the observation that there was detectable *ERCC1* transcript in the *ERCC1*^{*292} mice, we tested tissue extracts from *ERCC1*^{*292} mice and their wild-type litter-mates using ERCC1-specific antibodies; however, all the available antibodies, which were raised against the human ERCC1 protein, did not recognize the mouse protein. To test for expression of the antisense gene at the *ERCC1* locus, northern blot analysis of kidney and liver RNA was performed; a probe corresponding to the mouse genomic *ERCC1* 3′ region (probe C; see Fig. 1b) that hybridizes to the antisense mRNA revealed a transcript of 5–6 kb that was expressed in tissues of wild-type, *ERCC1*^{*292} and *ERCC1* knockout mice (data not shown), indicating that gene targeting did not alter the expression level of the antisense transcript.

Phenotype, frequency of recovery, and pathology of *ERCC1*-mutant mice

In order to investigate the effects of genetic background on embryonic lethality and life span, in addition to the C57Bl/6/129 hybrid *ERCC1* knockout and *ERCC1*^{*292} mice, whose generation we have described, we also generated FVB/129 hybrid *ERCC1*^{*292} mice. A number of the characteristics of *ERCC1* deficiency have been described by McWhir *et al.* [15], and are confirmed in both our

Figure 2

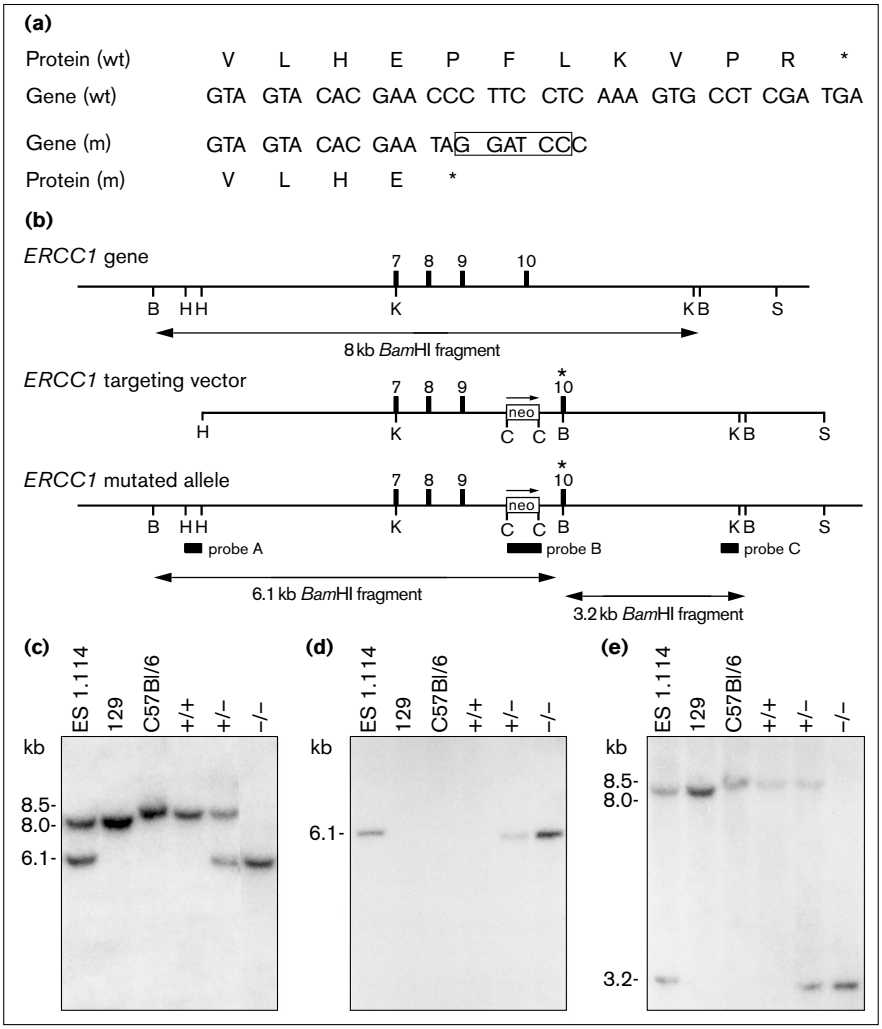

Disruption of the *ERCC1* gene: the *ERCC1*^{*292} mutation. **(a)** The nucleotide sequence and encoded protein sequence (in single-letter amino-acid code, with asterisks indicating stop codons) of the 3′ end of wild-type (wt) and mutant (m) murine *ERCC1*. An introduced diagnostic *BamH*I restriction site is boxed. **(b)** Strategy for introducing a stop codon into exon 10 of *ERCC1* by homologous recombination in ES cells. Part of the genomic structure of the *ERCC1* locus is depicted, annotated as for Figure 1b. The *neo* cassette was inserted into a *Cla*I restriction site that was generated by site-directed mutagenesis in intron 9. The diagnostic restriction site in exon 10 is indicated by an asterisk. Probe A detects a 6.1 kb and an 8 or 8.5 kb *Bam*HI fragment in the mutant and wild-type alleles, respectively. Probe C hybridizes to a 3.2 kb and an 8 or 8.5 kb *Bam*HI fragment in the mutant and wild-type alleles, respectively. **(c–e)** Southern blot analysis of *Bam*HI digested genomic DNA from ES clone 1.114 and 129 and C57Bl/6 mice, and tail DNA of the indicated genotypes, probed with probes (c) A, (d) B and (e) C.

ERCC1 knockout and *ERCC1*^{*292} mice. These include, for all *ERCC1*-mutant mice, irrespective of genetic background, a frequency of recovery of homozygous mutants far below Mendelian expectation (Table 1), a severely runted phenotype (Fig. 4) and a markedly reduced life span. Life span reduction was more severe in our *ERCC1* knockout mice (C57Bl/6 background) and the FVB-background *ERCC1*^{*292} mice, which had maximal ages of 38 days and 78 days, respectively; C57Bl/6-background *ERCC1*^{*292} mice had a life span of up to 6 months. The *ERCC1*-mutant mice reported by McWhir *et al.* [15] died between days 20 and 28. We also noted sex differences in phenotype for the C57Bl/6-background *ERCC1*^{*292} mice: male mice were more severely runted (only 25% of the weights of controls, compared with 30–50% for females) and had a shorter life span (data not shown).

We investigated when lethality (embryonic or *post partum*) occurred and whether these features were influenced by genetic background. Both *ERCC1* knockout and *ERCC1*^{*292} mice in a C57Bl/6/129 background revealed early embryonal lethality (by day 13.5 after gestation; Table 1), and growth delay was noted (data not shown). Interestingly, embryonal lethality was not seen in FVB/129-hybrid *ERCC1*^{*292} mice, although in this case many *ERCC1*-mutant animals died at a later stage — the same low frequency of homozygous mutant offspring was found for all F1 crosses at the time of genotyping (10 days *post partum*; Table 1). Together, our data suggest that, for the *ERCC1*^{*292} mutation, the genetic make-up influences the penetrance of *ERCC1* deficiency. All further characterizations were done in *ERCC1*^{*292} mice (and additionally in *ERCC1* knockouts where stated) in a C57Bl/6/129 hybrid background.

Detailed histological examination was performed on a total of 13 *ERCC1*^{*292} and *ERCC1* knockout mice, sacrificed when still in a good condition. We detected neither

Figure 3

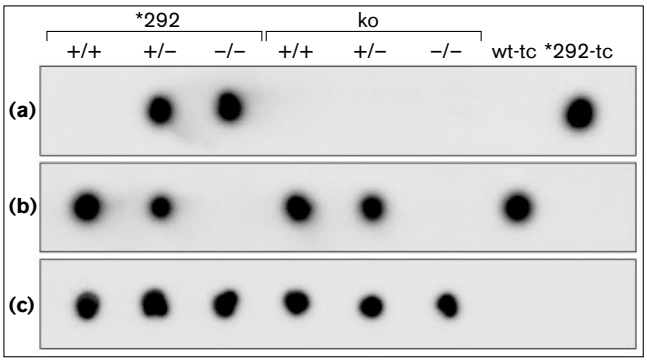

RT-PCR and dot-blot analysis of *ERCC1* transcripts. Exons 9 and 10 of the mouse *ERCC1* locus were amplified by RT-PCR (using total MEF RNA from embryos on embryonic day 13.5). Amplified DNA from homozygous wild-type (+/+), heterozygous (+/–) and homozygous mutant (–/–) offspring of both *ERCC1*^{*292} (*292) and *ERCC1* knockout (ko) F1 heterozygotes was dot-blotted and hybridized to labelled oligonucleotide probes specific for **(a)** *ERCC1*^{*292} (p81) and **(b)** wild-type *ERCC1* (p228). **(c)** As a control, amplimers specific for mouse *XPB* were added to the cDNA mix and amplified DNA was hybridized to an *XPB*-specific oligonucleotide probe (p73). As a control for the specificity of hybridization of the mutant and wild-type *ERCC1*-specific oligonucleotides, both wild-type (wt-tc) and *ERCC1*^{*292} (*292-tc) targeting constructs were also spotted.

Figure 4

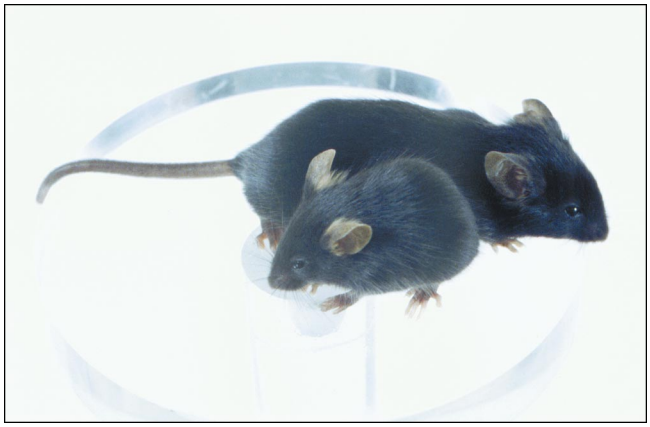

The *ERCC1*^{*292} mutation causes reduced growth. Homozygous wild-type (back) and homozygous mutant (front) 3–4 week old litter-mates (C57Bl/6/129 hybrid background) from a heterozygous *ERCC1*^{*292} intercross.

pathological abnormalities in the heart, lung, brain and eyes, nor any of the characteristics often found in XP patients, such as neurological abnormalities, premalignant lesions or immature sexual development (in mice up to 6 months old). By morphological criteria, the ovaries and testes, although proportionately small, looked normal: ovaries contained ova and follicles, sometimes with signs of cyclic changes, indicating normal pituitary regulatory function, and spermatogenesis also appeared normal. *ERCC1*^{*292} mice that reached the age of approximately 6 months, however, gave no progeny when mated with C57Bl/6 mice, suggesting that they were infertile. Figure 5 shows the histopathology of *ERCC1*^{*292} mice; identical results were obtained with *ERCC1* knockout mice (data not shown).

Table 1

Genotype of offspring and embryos derived from mice heterozygous for mutations in *ERCC1*.

Mutation	Age	+/+	+/–	–/–‡
ERCC1^{*292}*	Newborn	121 (35%)	210 (61%)	13 (4%)
	E13.5	17 (31.5%)	34 (63%)	3 (5.5%)
ERCC1^{*292}†	Newborn	25 (27%)	60 (65%)	7 (8%)
	E13.5	19 (23%)	42 (51%)	21 (26%)
ERCC1 knockout*	Newborn	32 (30%)	70 (63%)	8 (7%)
	E13.5	9 (24%)	24 (63%)	5 (13%)

Both embryos (from embryonic day E13.5) and neonates (10 days *post partum*) were genotyped by Southern blot analysis using probe A (see Fig. 1b); the numbers and proportions of homozygous wild-type (+/+), heterozygous (+/–) and homozygous mutant (–/–) mice are shown. *C57Bl/6/129 hybrid background. †FVB/129 hybrid background. ‡All –/– mice and embryos of both genotypes displayed severe growth retardation.

Previously, McWhir *et al.* [15] reported light-microscopically detectable abnormalities in liver nuclei of *ERCC1*-mutant mice. We observed similar nuclear abnormalities (Fig. 5d), but in addition, the kidney, skin and spleen were found to be abnormal. The skin of *ERCC1*^{*292} mice was thin and lacked subcutaneous fat (Fig. 5a,b). In the spleen of mutant mice at 3 weeks of age, an increased and early onset of ferritin deposition was found (Fig. 5c), which was absent from age-matched wild-type mice (data not shown). The peripheral blood in some samples showed an increase in Howel Jolly bodies (data not shown). The increase in ferritin deposition might point to an increased turnover of erythrocytes; however, there was no sign of overt haemochromatosis. In the kidney, we found dilated tubules containing leaked proteinaceous material (Fig. 5e), indicative of renal dysfunction, as well as nuclear abnormalities; these kidney abnormalities were not seen in wild-type litter-mates (data not shown).

Electron microscopy confirmed and extended the mutant-specific nuclear abnormalities in liver and kidney (seen in Fig. 5d,f and also McWhir *et al.* [15]): the chromatin was very coarse, and the nucleoli were more prominent than normal and showed an abnormal organization (Fig. 5g). Furthermore, nuclear invagination and intranuclear inclusions were observed (Fig. 5h). Flow cytometry of liver cells of young *ERCC1*^{*292} mice showed increasing octaploidy (Fig. 6a). The abnormal nuclear morphology was also reflected in the distribution of nuclear size, as revealed by nominal area measurements in liver sections (Fig. 6b).

Figure 5

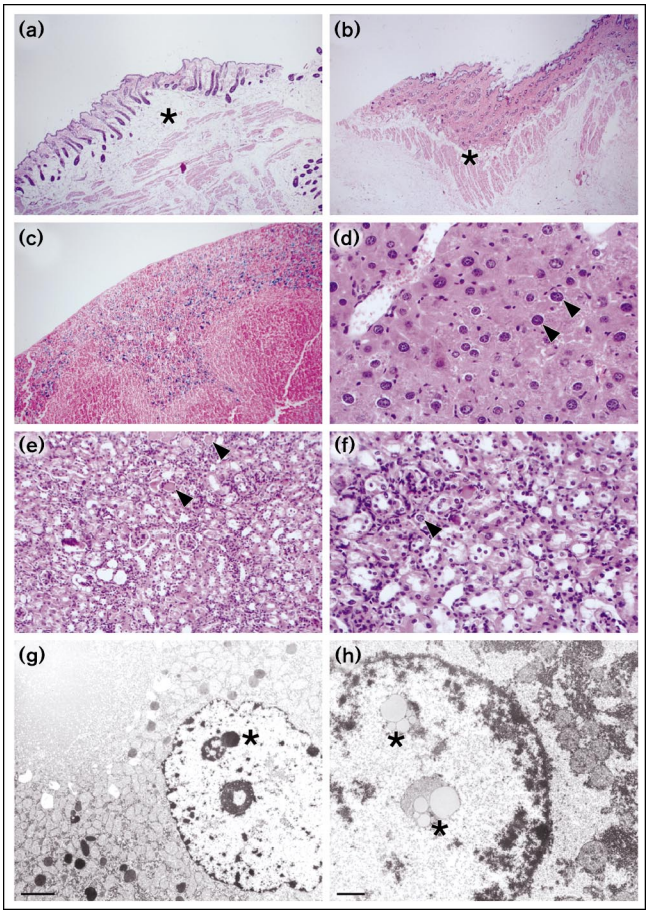

Histopathology of offspring of *ERCC1*^{*292} F1 heterozygotes at 3 weeks of age. Sections of the skin (18× magnification) of **(a)** homozygous wild-type and **(b)** homozygous mutant mice; note the absence of subcutaneous fat (indicated with asterisks) in homozygous mutant mice. **(c)** Section of the spleen (18× magnification) of a homozygous mutant mouse; note the ferritin staining (blue) in macrophages. **(d)** Liver section (haematoxylin-stained and eosin-stained; 270× magnification) of a homozygous mutant mouse showing anisokaryosis. Several aberrantly enlarged nuclei are indicated with arrowheads. **(e)** Kidney sections (haematoxylin-stained and eosin-stained; 66× magnification) of a homozygous mutant mouse showing dilated tubules occupied with leaked eosinophilic proteinaceous material (indicated with arrowheads). **(f)** Higher power view of a kidney section (270× magnification) showing aberrant nuclei (indicated with arrowheads). Electron-microscopical analysis of **(g)** kidney and **(h)** liver sections of a homozygous mutant mouse showing that the chromatin is very coarse. Nuclear inclusions are indicated with an asterisk: some inclusions are associated with nucleoli (see asterisk in (g)).

In order to find out whether excess programmed cell death was involved in the growth deficit associated with *ERCC1* mutation, serial-sectioned liver, kidney and spleen tissue were analyzed using the TUNEL assay [18]. No clear increase in TUNEL-positive nuclei was seen in the organs from *ERCC1*-mutant mice compared to those from wild-type litter-mates (data not shown). These results indicate that excessive apoptosis did not occur in *ERCC1*-mutant mice and suggest that the reduced size of these mice was due to either a reduction or an early halt to proliferation.

Growth and cell cycle properties of *ERCC1*-mutant fibroblasts

Because the reduced size of *ERCC1*-mutant mice suggested a potential role for *ERCC1* in cell proliferation, we measured growth rates of primary *ERCC1*^{*292} MEFs *in vitro*. Early-passage (passage 3) *ERCC1*-mutant MEFs grew about three times as slowly as wild-type fibroblasts; heterozygous MEFs had a doubling time of 36 hours compared with 24 hours for wild-type fibroblasts (Fig. 7a). Proliferation decreased with passage in culture and, by passage 6–7, fibroblasts from *ERCC1*^{*292} mice failed to divide, whereas MEFs from heterozygous and wild-type litter-mates grew quite rapidly (three independent cell lines of each genotype were tested). The homozygous mutant MEFs were larger than wild-type cells and contained giant polyploid nuclei (compare Fig. 7a and 7b). All MEFs showed contact inhibition, but monolayers of wild-type cells were more dense (1.45×10^5 cells per cm^2) than those of homozygous mutant MEFs (0.9×10^5 cells per cm^2). The reduced life span and rate of proliferation of *ERCC1*-mutant primary cells indicate an early onset of cellular replicative senescence in these cells. The difference in doubling time was partly due to a decrease in the number of dividing cells in *ERCC1*^{*292} cultures, as determined by incorporation of bromodeoxyuridine (BrdU) into chromosomal DNA during a 48 hour labelling period. Only 53% of passage 3 *ERCC1*^{*292} MEFs were actively cycling, compared with 91% of controls.

In order to analyze cell cycle properties, we pulse-labelled cells with BrdU for 1 hour, and followed their progression through the cell cycle. In the cycling population (which was close to 50% for *ERCC1*^{*292} fibroblasts), the relative distribution of cells in the different cell cycle phases was similar for *ERCC1*^{*292} cells and wild-type controls (Fig. 7c, curves with solid lines, –MMC). This indicates that cycling *ERCC1*-mutant MEFs do not accumulate at a specific stage of the cell cycle. Consistent with the finding that many *ERCC1*-mutant cells do not cycle, we find increased levels of p21$^{cip1/waf1}$ in *ERCC1*-mutant MEFs compared with wild type controls (by immunoblotting; data not shown). In order to examine whether untransformed *ERCC1*^{*292} MEFs exhibit a cell cycle arrest in response to DNA damage, the effect of treatment of *ERCC1*^{*292} MEFs with DNA-damaging agents was investigated. Following treatment with a low dose of the cross-linking agent mitomycin C (MMC), homozygous mutant MEFs, but not wild-type (repair-proficient) MEFs, exhibited a DNA-damage-induced delay in G2 (Fig. 7c, dashed lines, +MMC), consistent with *ERCC1*-mutant MEFs having both a cross-link repair defect and a normal G2 cell cycle arrest mechanism. Cytogenetic analysis of *ERCC1*-mutant MEFs revealed a normal karyotype and no detectable

Figure 6

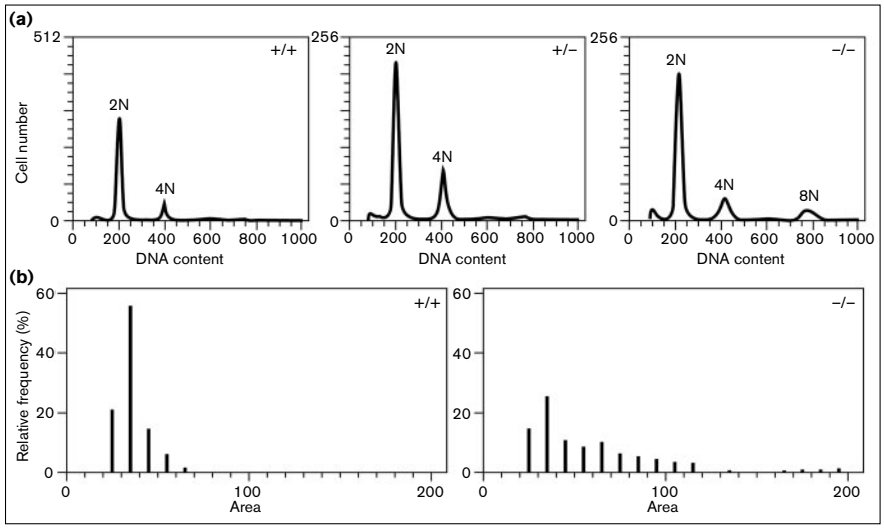

(a) Liver cells from homozygous wild-type (+/+), heterozygous (+/–) and homozygous mutant (–/–) offspring (17–20 days old) of *ERCC1*^{*292} F1 heterozygotes were isolated and the DNA content was determined by flow cytometry after DNA staining with propidium iodine. The positions of peaks for 2N, 4N and 8N DNA content are shown on the histograms. **(b)** Morphometric analysis of *ERCC1*^{*292} liver nuclei. Histograms show the nominal areas of nuclei for a wild-type and homozygous mutant animal, illustrating the range of enlarged nuclei.

increase of chromosomal breaks, gaps and abberations compared with wild-type controls (data not shown).

DNA repair parameters of *ERCC1*-mutant fibroblasts

McWhir *et al.* [15] reported increased UV sensitivity and reduced incision and dimer removal after UV exposure for cells derived from their *ERCC1*-deficient mouse mutant. In order to extend these findings, we analyzed DNA repair and incision using an assay for UV-induced unscheduled DNA synthesis (UDS) of primary MEFs (three independent cell lines from each genotype). UDS in *ERCC1*^{*292} cells was extremely low (4% of that of wild-type cells; Fig. 8). Interestingly, fibroblasts from heterozygous litter-mates showed a slight, but significant, reduction in UDS (to a level of 73% that of wild-type controls). Similar results were obtained with *ERCC1* knockout cells (data not shown).

As an estimate of another repair parameter, we measured cell survival after exposure to various genotoxic agents. In addition to the UV sensitivity (Fig. 9a) we investigated sensitivity to DNA cross-linking agents. A hallmark of chinese hamster ovary cell lines that contain mutations in *ERCC1* (or *ERCC4*) is their extreme sensitivity (80–100-fold above controls) to cross-linking agents, presumably

Figure 7

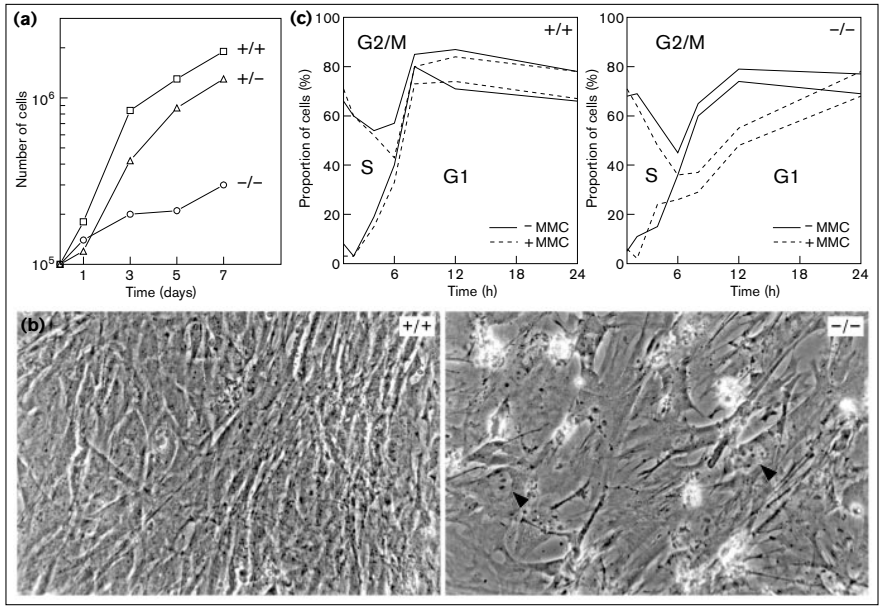

(a) Growth kinetics of primary fibroblasts. Passage-3 MEFs (10^5) from wild-type (+/+), heterozygous (+/–) and homozygous mutant (–/–) offspring of *ERCC1*^{*292} F1 heterozygotes were plated in 60 mm culture dishes. Doubling times were calculated from the exponential portion of the curve to be approximately 24 h, 36 h and 73 h for +/+, +/– and –/– MEFs, respectively. **(b)** Microscopical analysis (phase contrast; magnification 16×) of MEFs from *ERCC1*^{*292} mice and wild-type litter-mate controls. Wild-type MEFs reached a two-fold higher saturation density compared with *ERCC1*-mutant fibroblasts. Arrowheads point to giant nuclei. **(c)** Cell cycle progression of S phase wild-type and *ERCC1*^{*292} MEFs after a 1 h pulse with bromodeoxyuridine (BrdU) and with and without treatment with 0.4 μg ml^{-1} mitomycin C (MMC). The percentage of G1, S and G2/M phase cells among the cycling population (BrdU-positive) was quantified and is presented in the form of area plots, in which the percentages of cells in each cell cycle phase are plotted against time.

Figure 8

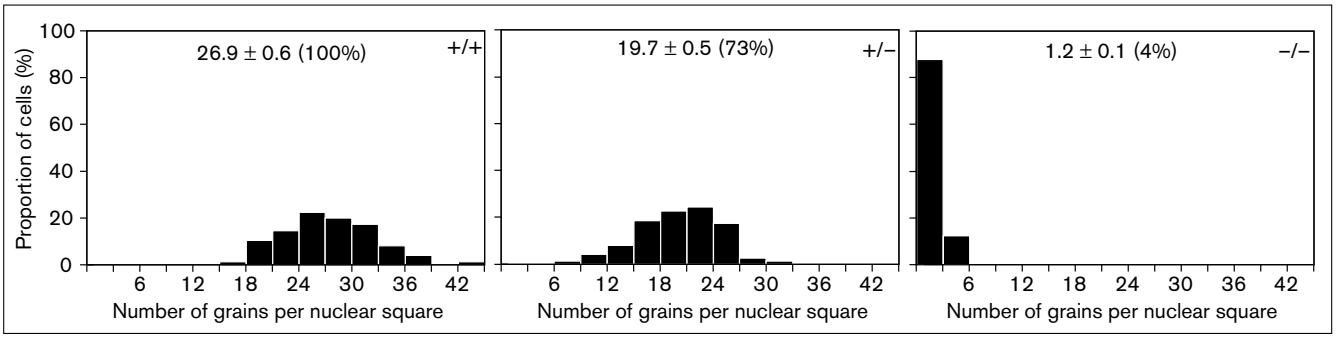

DNA repair capacity of MEFs from homozygous wild-type (+/+), heterozygous (+/–) and homozygous mutant (–/–) offspring of *ERCC1*^{*292} F1 heterozygotes. Histograms of UDS are shown, indicating the average UDS as a value and as a percentage of the wild-type control value.

reflecting the role of the ERCC1 complex in recombinational repair. As shown in Figure 9b, most *ERCC1*-mutant MEFs displayed a clear sensitivity to MMC, but a small fraction seemed resistant to MMC concentrations over a wide range. Comparable survival curves were obtained when another cross-linking agent, cisplatin, was used (data not shown), ruling out the possibility of a defect in drug metabolism. Moreover, when we examined the survival of the *ERCC1*-mutant MEFs after treatment with 7,12-dimethylbenz[a]anthracene (DMBA), a chemical agent that causes only bulky adducts, which are substrates for NER, a profound sensitivity was found (Fig. 9c) that was in the same range as that for *XPA*$^{-/-}$ cells [19]. No resistant cell population was apparent, however, indicating that the resistance is specific to the removal of cross-linking lesions, which are largely eliminated by recombinational repair.

A possible explanation for the *ERCC1*-mutant cell population resistant to DNA cross-linking is the existence of another recombination repair process (for example, homology-dependent recombination repair) active only at a specific stage of the cell cycle and requiring cell cycle arrest. As shown in Figure 7c, the mechanism of damage-induced G2 cell cycle arrest is still functional in the *ERCC1*-mutant MEFs. Unfortunately, the limited lifespan of the primary MEFs precluded retesting of the resistant cell fraction for MMC sensitivity. A similar bimodal behaviour was found, however, for some chinese hamster ovary NER mutants: in this case, the resistant fraction showed the same survival as the original cell population (data not shown), consistent with the explanations given above. Transfection of immortalized mouse *ERCC1*^{*292} fibroblasts with wild-type human *ERCC1* cDNA fully complemented the UV sensitivity (Fig. 9d), indicating that the repair defect is the

Figure 9

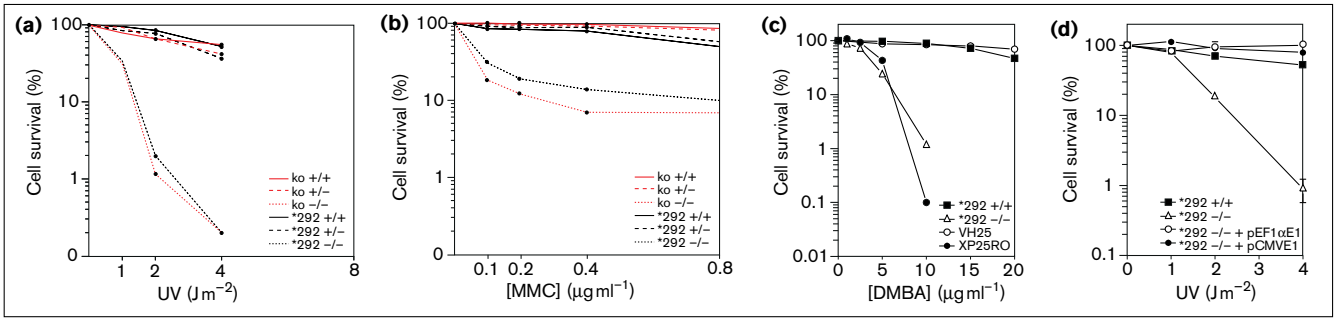

Cell survival of primary MEFs derived from offspring of *ERCC1*^{*292} (*292) and *ERCC1* knockout (ko) F1 heterozygotes after exposure to genotoxic agents. Survival of homozygous wild-type (+/+), heterozygous (+/–) and homozygous mutant (–/–) cells after exposure to **(a)** UV and **(b)** a 1 h pulse of MMC. Each value is the mean of the survivals of three independent MEF cell lines, tested in duplicate. **(c)** Survival of cells from *ERCC1*^{*292} mutant mice and wild-type littermates after exposure to 7,12-dimethylbenz[a]anthracene (DMBA). The normal human fibroblasts VH25 and the human XP cell line, XP25RO (XP-A complementation group), were included as controls. The DMBA survival of *XPA*$^{-/-}$ MEFs is identical to that of XP25RO cells (unpublished observations). **(d)** Survival, following UV exposure, of *ERCC1*-mutant MEFs transfected with the human *ERCC1* minigene constructs pEF1αE1 and pCMVE1, which contain wild-type human *ERCC1* cDNA driven by the human elongation factor-1α and CMV promoters, respectively. Points are average values for duplicate wells (± SEM).

Figure 10

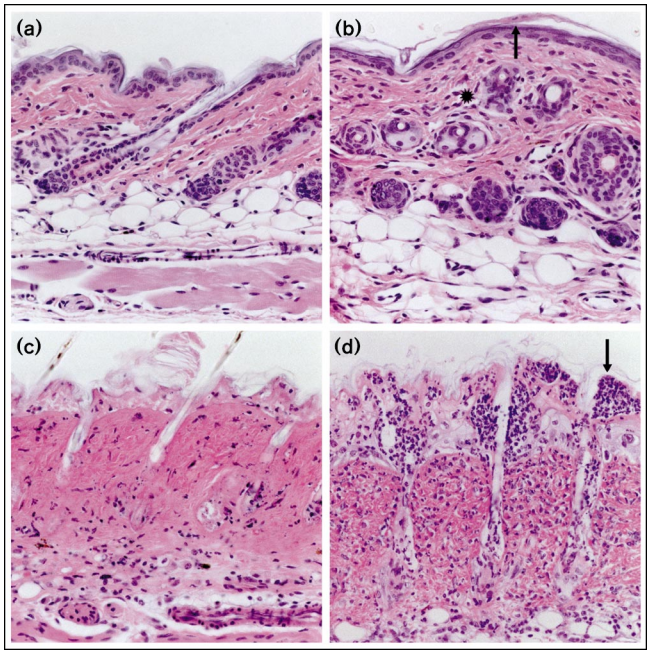

Acute effects in the skin of *ERCC1*^{*292} and *XPA*$^{-/-}$ mice after treatment with DMBA. Shaved mice (3 weeks of age) were treated with a single dose of 30 μg DMBA. Three days after treatment, part of either the exposed skin or untreated skin from dead *ERCC1*^{*292}-mutant mice or sacrificed control animals was sampled and processed for histopathology; skin is shown at 270× magnification. **(a)** Untreated skin from wild-type litter-mates of *ERCC1*^{*292} mice. The effects of DMBA treatment on **(b)** wild-type litter-mates of *ERCC1*^{*292} mice and **(c)** *ERCC1*^{*292} mice. Hardly any epidermal changes are detectable for wild-type mice: a minimal influx of inflammatory cells is noted (indicated with an asterisk), as are signs of parakeratosis (indicated with an arrow). In treated *ERCC1*^{*292} mice, the dermal as well as epidermal changes are severe and characterized by massive necrosis of epidermis and papillary dermis, and a minimal influx of inflammatory cells in the dermis and epidermis. **(d)** Treated skin from *XPA*$^{-/-}$ mice. Dermal as well as epidermal changes are noticeable and characterized by epidermal degeneration, necrosis and pustule formation (indicated with an arrow) and a marked influx of inflammatory cells in dermis and epidermis.

result of *ERCC1* targeting. From this set of experiments, we conclude that both the *ERCC1* knockout and *ERCC1*^{*292} mice have a severe NER defect and a deficiency in cross-link repair.

Carcinogenicity studies

In order to establish whether the *ERCC1*^{*292} mice are susceptible to developing skin cancer, four three-week-old mutant mice were exposed to 30 μg DMBA, followed by a promotion protocol (2.5 μg TPA administration twice a week). As a control, both heterozygous and wild-type litter-mates (20 of each) were divided into four groups, each receiving 0, 5, 15 or 30 μg DMBA, followed by the TPA treatment. The dose given to *ERCC1*-mutant mice was chosen because *XPA*$^{-/-}$ mice, which are also totally NER-deficient, treated with the same dose showed only reversible skin abnormalities (Fig. 10d). However, treated *ERCC1*-mutant mice displayed massive epidermal necrosis and minimal infiltration of leucocytes (Fig. 10c). All *ERCC1*-mutant mice died three days after the first administration of DMBA, whereas *XPA*$^{-/-}$ mice appeared normal (both strains are in the same 129/C57Bl/6 hybrid genetic background). These data indicate that *ERCC1*-mutant mice are much more sensitive to DMBA than are *XPA*$^{-/-}$ mice, which is in contrast to the corresponding MEFs, which are equally DMBA-sensitive (Fig. 9c). Importantly, mice heterozygous for the *ERCC1*^{*292} allele did also not display increased DMBA sensitivity, nor (36 weeks after the start of the DMBA-treatment) a clear cancer predisposition (data not shown). Both homozygous wild-type (28/63) and heterozygous (23/63) DMBA-treated mice developed one or more papillomas. Tumour DNA of heterozygotes was analyzed by Southern blotting, but there was no evidence for loss of heterozygosity of the wild-type *ERCC1* allele (data not shown), indicating that loss of the remaining functional allele — and thereby inactivation of the two DNA repair pathways — does not provide a selective advantage for tumour development.

Discussion

Comparison of the *ERCC1* knockout and *ERCC1*^{*292} alleles at the molecular and phenotypical level

Besides its involvement in NER, the ERCC1–XPF endonuclease is also implicated in the repair of cross-links, most likely *via* a mitotic recombination repair pathway. Consequently, a defect in this gene is expected to cause a combination of features derived from deficiencies in both systems. Our previous mutational analysis of ERCC1 has shown that many of the alterations to the middle part of the protein render it unstable, presumably by impairment of the stabilizing interaction with XPF [14]. On the other hand, deletion of five or six carboxy-terminal amino acids affects both ERCC1 repair functions but does not dramatically destabilize the protein [14]. In addition, we found that a low level of ERCC1–XPF may be sufficient for the repair of very genotoxic DNA cross-links, but not for NER [14]. In view of the dual function of the protein and the notion that its total inactivation results in a very severe phenotype [15], we decided to generate two types of *ERCC1*-mutant mouse model: an *ERCC1* knockout mouse, and one in which the ERCC1 protein contained a seven amino acid carboxy-terminal truncation (equivalent to deleting six residues of the human protein). In RT-PCR experiments using *ERCC1* knockout MEFs, no *ERCC1* mRNA could be detected. This excludes the possibility of dominant-negative effects of a truncated ERCC1 protein and indicates that the knockouts represent true null mutants. In contrast, RNA expression was detected for the *ERCC1*^{*292} allele, but the level of transcript was only about 15% of the expected level, probably as a consequence of the marker insertion

and/or the mutation. MEFs heterozygous for *ERCC1*^{*292} revealed a small but significant reduction (27%) in UV-induced UDS (Fig. 8). Independently, McWhir *et al.* [15] reported a similar decrease in the level of incision and an accumulation of DNA breaks in MEFs heterozygous for a mutation in *ERCC1*. These findings point to haplo-insufficiency — the normal NER capacity is diminished when there is only one functional *ERCC1* allele. This suggests that, under normal conditions, ERCC1 is a rate-limiting factor in NER of MEFs.

Both at the cellular level and at the level of the organism, the *ERCC1* knockout and *ERCC1*^{*292} phenotypes are very alike and each mutation has a dramatic effect on NER. In view of the anticipated partial stability of the ERCC1^{*292} protein, and the fact that it still harboured the intact UvrC-homologous domain, the *ERCC1*^{*292} mice might have displayed a partial defect in cross-link repair. This was not found, however. Therefore, protein truncation as well as reduced transcript levels may have made the *ERCC1*^{*292} phenotype more severe than anticipated. The major phenotypic difference between the *ERCC1* knockout and *ERCC1*^{*292}-mutant mice, however, seemed to be in the life span. The *ERCC1* knockout mice all died before day 38, whereas the maximum life span of *ERCC1*^{*292} mutants was considerably longer (6 months). All the *ERCC1*-mutant mice described by McWhir and coworkers [15] died even earlier than our knockout mutants, between days 20 and 28. Furthermore, we showed that both genetic background and sex influenced the penetrance of embryonal and perinatal lethality and of lifespan alterations.

Comparison with other NER-deficient mouse models and genotype–phenotype correlations

The consequences for the mouse of a defect solely in NER are apparent from the *XPA* knockout mouse. *XPA*$^{-/-}$ mice are viable, develop normally and have a normal life span, but are photosensitive and predisposed to UV-induced skin cancer and ocular tumours [19,20]. *XPA*$^{-/-}$ MEFs have a total NER deficiency and are hypersensitive to UV and DMBA [19,20]. The effects of NER loss — confirmed by the phenotype of the *XPC* knockout mice, which have a specific defect in the global genome repair subpathway of NER [21,22] — are mild compared with the effects of *ERCC1*^{*292}. McWhir *et al.* [15] proposed accumulation of an endogenously generated NER lesion as the cause of the *ERCC1*-mutant features. As the NER defect in *XPA* null and *ERCC1* null mutants is the same, however, this explanation has become unlikely. Instead, we infer that in the *ERCC1*^{*292} mice, the extra pathological characteristics, which lack a parallel in the human XP patients, must be due to the additional *ERCC1* function. Thus, the liver, kidney and spleen manifestations, as well as the developmental delay and reduced life span, are most probably derived from impairment of the interstrand cross-link repair pathway. The same holds true at the cellular level for the striking features of the *ERCC1*-mutant MEFs; namely the nuclear abnormalities (including enlarged polyploid nuclei and nuclear inclusions) and, importantly, replicative senescence.

How can we explain the 'non NER' clinical manifestations in terms of inactivation of ERCC1-dependent cross-link repair? The liver and kidney malfunctions are probably the consequence of the prominent nuclear abnormalities seen in these organs. Polyploid nuclei normally develop later in life, but are already apparent at, or soon after, birth in *ERCC1*-mutant mice. Other indications also point to premature senescence, such as the occurrence of eosinophilic nuclear inclusions, which have frequently been observed in cells of ageing animals [23]. In addition, the striking early onset of a proliferative arrest of *ERCC1*^{*292} MEFs (with a concomitant increase in p21$^{cip1/waf1}$), which is due to the presence of a large proportion of cells arrested in the cell cycle, is a hallmark of replicative senescence (see [24] for a recent overview). The early stop in cellular proliferation may also explain the severe reduction in weight, the poor and delayed development, and early death. Thus, *ERCC1*-mutant mice display several signs of premature senescence. What is the relationship between premature senescence and impaired cross-link repair? The involvement of defective cross-link repair suggests that accumulation of interstrand cross-links causes the observed phenomena. Candidates for endogenous agents inducing such lesions are mutagenic carbonyl compounds such as malondialdehyde (MDA), which is the major by-product of arachidonic acid metabolism and lipid peroxidation [25]. MDA produces adducts (mainly at deoxyguanosine) and induces interstrand cross-links, which have been detected in liver DNA, for example, and have been implicated in carcinogenesis [25].

Persistent DNA damage triggers p53 accumulation, which in turn induces cell cycle arrest, thereby providing a time-window for DNA repair and the prevention of mutagenesis [26]. Moreover, p53 has been implicated in a spindle checkpoint that controls the ploidy of cells [27]. One of the most important downstream effectors induced by p53 is the cell cycle inhibitor p21$^{cip1/waf1}$ [28], which has also been associated with cell differentiation and senescence. The involvement of p21$^{cip1/waf1}$ in the ERCC1-dependent cross-link repair pathway is strongly supported by the striking resemblance of *ERCC1*^{*292} mice to transgenic mice that express high levels of p21$^{cip1/waf1}$ in the liver [29]. These mice display dramatically inhibited hepatocyte proliferation, resulting in aberrant tissue organization, runted liver and body growth and increased mortality; furthermore, large polyploid nuclei were observed, also suggesting arrest during the G2 phase of the cell cycle [29].

The body of evidence for the involvement of p21$^{cip1/waf1}$ and p53 in ERCC1-dependent cross-link repair is

compelling: first, as mentioned before, we find higher levels of p21$^{cip1/waf1}$ in untreated *ERCC1*^{*292} MEFs than in wild-type controls; second, McWhir and coworkers [15] have shown accumulation of p53 in liver, kidney and brain of *ERCC1*-mutant mice; and third, under certain conditions, p53 activation triggers apoptosis in response to DNA damage [30], although overexpression of p21$^{cip1/waf1}$ in liver cells does not lead to increased apoptosis [29]. Similarly, we failed to detect high levels of apoptosis in either *ERCC1*-mutant mice or cultured *ERCC1*-mutant MEFs (data not shown). In summary, our data, supported by many independent findings, suggest that very genotoxic lesions, such as MDA-induced DNA cross-links, which are normally targeted by the ERCC1-dependent recombination pathway, accumulate at a high rate in *ERCC1*-mutant mice, and activate p53. In turn, p53 induces p21$^{cip1/waf1}$, resulting in early cell cycle arrest, nuclear polyploidy and other cellular abnormalities. These features of premature senescence cause liver and kidney malfunction, arrested development and early death. Thus, endogenously generated cross-links may be an important factor in the process of ageing, and ERCC1-dependent recombination may constitute a critical barrier against senescence.

ERCC1 and human repair syndromes

ERCC1 is one of the few NER genes for which no corresponding human (repair) disorder is known. This may be due to the severe consequences of *ERCC1* inactivation, which cause prenatal or early postnatal death. As in the case of the XPF subunit of the ERCC1/XPF endonuclease, a mutation affecting only the NER function, but leaving sufficient amounts of complex for its role in cross-link repair, is expected to give a phenotype very similar to that of XP-F patients [7,14]. The XP-F complementation group is characterized by relatively mild XP features, with late onset of symptoms. Fibroblasts from XP-F patients still perform a low level (15–20%) of DNA repair [31]. Apparently, the low concentration of the ERCC1–XPF complex in these cells is rate-limiting for NER but still permits some repair to occur. This concentration may be sufficient to cope with a low steady-state DNA-damage load. Moreover, for high UV doses, a low but long-lasting type of repair activity has been observed in XP-F cells [32]. In the end, this may still permit removal of a considerable fraction of the lesions.

The phenotype of the *ERCC1*-mutant mice described here may provide clues for a corresponding syndrome in man resulting from a more severe impairment of *ERCC1* function. In extrapolating to man, it should be kept in mind that, except for the repair parameters, the genetic background in mice already appears to have a significant effect on the penetrance and expressivity of the clinical features. With this caveat in mind, rare genetically heterogeneous, autosomal recessive disorders such as Roberts syndrome may be considered potential candidates for an *ERCC1* defect. Roberts syndrome patients display a variety of developmental anomalies, including renal defects and malignancies. Interestingly, some patients exhibit, at the cellular level, nuclear (heterochromatin) abnormalities and UV sensitivity as well as cross-link sensitivity [33]. In one Roberts syndrome patient, we failed to find defects in *ERCC1* at either the DNA or RNA level (data not shown); however, this does not exclude *ERCC1* mutations in other cases. Very recently, we have identified an XP patient with a mutation assigned to the XPF component of the dual functional ERCC1/XPF endonuclease who has a number of unusual features including growth defects and premature senescence, indicating the existence of further parallels between the mouse *ERCC1*-mutant system and human syndromes (our unpublished observations). A more versatile experimental animal model for *ERCC1* deficiencies, which might direct assignment of the clinical parameters to the different ERCC1 activities, awaits the generation of mouse mutants with specific defects in each of the *ERCC1* functions.

Materials and methods

Targeting constructs and disruption of ERCC1 *in ES cells*

Genomic *ERCC1* fragments were obtained by screening a 129/CCE EMBL4 genomic library (kindly provided by G. Grosveld) with a murine *ERCC1* cDNA [19]. A knockout targeting construct was prepared by subcloning a ~9.5 kb *Hin*dIII/*Sal*I fragment containing murine *ERCC1* exons 6–10 into pBR322. A unique *Cla*I restriction site was generated in exon 7 by uracil-DNA-mediated mutagenesis as described before [34], using primer p89 (5′ TCCAGCTTATCGATAAGGAGGT). The pMC1-*neo* resistance gene [16], containing a diagnostic *Bam*HI restriction site, was inserted into the unique *Cla*I site, yielding pE1NEO7. The *ERCC1*^{*292} targeting construct was generated as follows. A 2.8 kb *Kpn*I/*Xba*I fragment containing *ERCC1* murine exons 7–10 was subcloned into pTZ19 (Pharmacia). Using site-directed mutagenesis as described above, a stop codon was introduced into mouse *ERCC1* exon 10, deleting the amino-terminal 7 amino acids, using primer p81 (5′ GGCACTTTGAGGGATCC-TATTCGTGTAGTACT). In addition, we introduced a unique *Cla*I restriction site in intron 9, approximately 350 bp upstream of exon 10, in order to insert the pMC1-*neo* resistance gene, using primer p82 (5′ TAGTACATCGATGGGCGG). All critical regions were confirmed by double-stranded-DNA sequence analysis [35].

The targeting constructs were separated from vector sequences by gel electrophoresis, purified by electroelution and introduced into 129/Ola-derived ES cells by electroporation (E14 cells were kindly provided by A. Berns and H. te Riele). Routinely, 1×10^7 cells were electroporated in ES medium, supplemented with fetal calf serum (FCS) and containing 10–15 μg linearized targeting vector, at 585 V cm^{-1}, 1200 μF, for 10 msec using a Progenetor II PG200 gene pulser (Hoeffer). Cells were seeded onto gelatin-coated 10 cm dishes (10^6 cells per plate) and, after 24 h, subjected to neomycin selection (200 μg ml^{-1}) in Dulbeccos' modified Eagles medium (DMEM) containing 60% Buffalo rat liver conditioned medium (BRL) [36] and supplemented with 10% FCS, 1% non-essential amino acids, 0.1 mM 2-mercaptoethanol and LIF (1000 units ml^{-1}; Gibco). After 6–7 days, individual G418-resistant clones were picked into 24-well dishes (Costar) and expanded (no feeder layer). Half of the cells in the 24-well dish was expanded and frozen at −80°C, and the other half was used to identify targeted events. Chromosomal DNA was extracted from expanded cultures as described previously [37], digested with *Bam*HI, and analyzed by Southern blot

analysis using probe A (a genomic 5′ ~0.3 kb *Hin*dIII fragment containing intron sequences flanking the targeting construct. Targeted clones were reconfirmed using probe C (an internal 3′ ~1.2 kb *Xba*I/*Kpn*I fragment 3′ of the *ERCC1* gene) and probe B (a probe covering the *neo* coding region) (see Fig. 1). All homologous recombinants showed bands diagnostic for correct integration of the *neo* marker without random integration of additional copies of the targeting construct. In case of the *ERCC1*^{*292} mutation, two independent ES clones were analyzed by RT-PCR. Mouse *ERCC1* cDNA harbouring the *ERCC1*^{*292} mutation was subjected to RT-PCR using primers p141 (5′ TTGTTCAAGTGGATG) and p92 (5′ CTGGGCATGGAAAATTC) to amplify the region covering the mouse *ERCC1* gene that was part of the targeting construct. The PCR fragment was subcloned into an M13mp18-cloning vector and individual clones were analyzed by replica-plating using mutant-specific p81 primer and wild-type-specific p228 primer (5′ GGCACTTTGAGGAAGGGTTCGTGTAGTACT). Two ES cell lines from each targeting experiment were used for blastocyst injection.

The complete 1.1 kb human *ERCC1* cDNA fragment was inserted into the pBluescript vector KS$^+$ (Stratagene). A ~2.4 kb human elongation factor-1α (EF1α) promoter fragment [38], including the first intron, was inserted into the 5′-end of this construct. The 2.4 kb poly(A) fragment of the human β-globin was inserted in the 3′-end of this construct, yielding peF1αE1. The plasmid pCMVE1 is similar to peF1αE1, but contains the CMV promoter instead of the EF1α promoter.

Generation of ERCC1*-mutant mice and culturing of MEFs*

Chimeric mice were obtained by injecting 10–15 ES cells of the two different types of *ERCC1*-mutant clones into C57Bl/6 blastocysts. ES cells were karyotyped before injection. An average of 8 blastocysts was transferred into pseudopregnant female recipient BCBA mice. Male chimeras were bred to C57Bl/6 animals to generate the *ERCC1*-mutant mice described in this study. In addition, male chimeras were also bred to FVB animals to investigate the effects of genetic background on embryonic lethality and lifespan. Targeted ES cell clones produced male chimeras whose germline transmitted the agouti coat colour marker in nearly all offspring. Homozygous *ERCC1*-mutant mice were obtained by intercrossing F1 heterozygotes. Southern blot analysis of tail DNA (using probe A; Fig. 1a) was used to genotype the offspring, using standard conditions.

MEFs were isolated from day 12–13 embryos. Part of the embryo was used for genotyping. The remaining embryonic tissue was minced using a pair of scissors and immersed in a thin layer of F10/DMEM culture medium supplemented with 10% FCS and antibiotics. After 24 h, 5 ml culture medium was added and after 4–5 days, the culture was trypsinized and cultured up to passage 6–9. Spontaneous immortalized cell lines were obtained by continuous subculturing of primary MEFs. DNA transfections of immortalized MEFs were performed using lipofectin (Gibco).

UDS, survival assays and in vivo *DMBA treatment*

For UDS testing, fibroblasts (passage 4–6) were seeded onto coverslips at day zero. The next day, cells were washed with phosphate-buffered saline (PBS) and irradiated with 16 J m^{-2} UV-C (Philips, TUV lamp). Subsequently, cells were incubated for 2.5 h in culture medium containing 10 μCi ml^{-1} [^{3}H]thymidine (50 Ci mmol^{-1}; Amersham), fixed and subjected to autoradiography as described before [39].

For survival assays, primary MEF cultures were exposed to UV or incubated with MMC for 1 h and allowed to grow for another 4–5 days before reaching confluency. Cells were labelled with [^{3}H]thymidine as described above, rinsed thoroughly with PBS and lysed in 0.2 M NaOH. The number of proliferating cells in each dish was estimated by scintillation counting of the radioactivity incorporated during a 3 h pulse-labelling. Cell survival was expressed as the ratio of irradiated over unirradiated cells. For DMBA treatment, cells were incubated with DMBA-containing medium for 2 h on day one. To activate DMBA, a microsomal S9-fraction (TNO-voeding, Zeist) was added. Cells were washed twice and grown until day six. Cell survival was measured by addition of the tetrazolium salt XTT (final concentration 0.12 mg ml^{-1}) to the culture medium. The amount of formazan dye formed after 2 h incubation was measured using an enzyme-linked immunosorbent assay reader, as described by the manufacturer (Boehringer).

For the *in vivo* DMBA experiment, about four weeks after birth, 20 ERCC1$^{+/+}$ and 20 ERCC1$^{+/-}$ mice were treated once a week on the shaved back with 0, 5, 15 and 30 μg DMBA dissolved in 100 μl acetone; *ERCC1*$^{-/-}$ mice (4) received only the 30 μg DMBA treatment. After DMBA treatment, the mice received the phorbol ester TPA (2.5 μg in 100 μl acetone) twice a week for twenty weeks.

Histological studies and electron microscopical analysis

Before postmortem examination, all animals were sacrificed by cervical dislocation. Tissues were fixed in 10% neutral buffered formalin. Following appropriate fixation times, tissues were trimmed, dehydrated through ascending grades of ethyl alcohol, cleared in xylene, and infiltrated with paraffin wax. Tissue sections of 4 μm were prepared and stained with haematoxylin and eosin. Ferritin staining was performed as described by Simpson *et al.* [40]. Sections (4 μm) were cut and stained with haematoxylin and eosin and Perls's for iron. For electron microscopy, liver and kidney were fixed in a mixture of glutaraldehyde (1.5%) and paraformaldehyde (1.5%) in phosphate buffer at pH 7.3. Organs were post-fixed in 1% OsO_4, 1.5% potassium hexanoferrate, rinsed in cacodylate and 0.2 M sodium maleate buffers (pH 6.0), and block-stained with 1% uranyl acetate. Following dehydration, tissues were embedded in Epon.

Flow cytometry and morphometric measurements

Replicative DNA synthesis and DNA content were analyzed using bivariate flow cytometry according to established protocols [41]. Liver cells were stained with propidium iodine and analyzed on a FACScan cytometer using the Lysis II program (Becton-Dickinson). For cell cycle analysis, exponentially growing passage-3 MEFs were labelled with 10 μM BrdU (Boehringer) at 37°C for 1 h and then mock-treated or incubated with MMC (0.4 μg ml^{-1} for 1 h). After the chase period, cells were fixed with 75% ethanol. Fixed cells were treated with 0.1 M HCl containing 0.5% Triton X-100, followed by heating at 95°C and rapid cooling to denature DNA. Cells were then incubated with florescein isothiocyanate-conjugated anti-BrdU antibodies (Boehringer) and counter stained with 2 μg ml^{-1} propidium iodine. For morphometric measurement of the nuclear diameters, 3 μm-thick sections were stained according to Mayer. Automated image analysis was carried out using a Zeiss large research microscope fitted with a Bosch monochromatic camera connected to a Kontron IBAS 2000 image analysis system (Kontron Bildanalyse). A 6.3× objective was used, giving a measurement field on liver section of 2.8 mm^2, which was enlarged 100× on the instrument monitor to give 306 pixels mm^{-1} of original image.

Reverse transcription PCR and dot-blot analysis

Total RNA was isolated from tissues by the LiCl/urea method [42]. The RNA was used for preparing cDNA with *ERCC1*-specific primers. Amplification was performed by 30 cycles of, consecutively, 2 min denaturing at 95°C, 2 min annealing at around 50°C and 3 min extension at 70°C. Amplified DNA was spotted onto nitrocellulose filters and hybridized to wild-type and mutant ^{32}P-labelled primers. Mutation detection was performed by RT-PCR on RNA isolated from day E13.5 MEFs. A 3′ mouse *ERCC1* cDNA fragment was amplified by PCR with oligonucleotides p1 (5′ CCTTATGCCCGGGCCTGGGCCCAC) and p2 (5′ TTATTGTGACATGGGCTAGGTGGC). Amplified DNA was spotted on nitrocellulose filters and hybridized with labelled oligonucleotide probes p81 (specific for the *ERCC1*^{*292} mutation) and p228 (wild-type-specific; 5′ GGCACTTTGAGGAAGGGTTCGTGTAGTACT). To assure that the samples were equally capable of undergoing amplification of specific sequences by the PCR method, amplimers specific for the mouse *XPB* gene – p108 (5′ CGACGCTGTGGCACCATGAG) and p73 (5′ AACCTAGGACCCACGAAGG) – were added to the cDNA mix and hybridized to a mouse *XPB* specific primer, p30 (5′ GCTGCCTGGATCCGTG).

Acknowledgements

We thank C.Th.M. van Oostrom for excellent technical assistance, M. Kuit for photography, L.J. Niedernhofer and N.G.J. Jaspers for sharing unpublished results, R.W. Hendriks for help with FACS analysis and P.M. Dortant for histological sample preparation. This work was supported by grants from the Dutch Cancer Society (projects EUR 90–20, 94–763) and a fellowship of the Royal Netherlands Academy of Arts and Sciences to G.W.

References

1. Friedberg EC, Walker GC, Siede W: *DNA Repair and Mutagenesis*. Washington, DC: ASM Press; 1995.
2. Bootsma D, Cleaver JE, Kraemer KH, Hoeijmakers JHJ: **Nucleotide excision repair syndromes: xeroderma pigmentosum, Cockayne syndrome and trichothiodystrophy.** In *The Metabolic Basis of Inherited Disease*, 8th edn. Edited by Scriver CR, Beaudet AL, Sly WS, Vall D. New York: McGraw-Hill; 1997: in press.
3. Hoeijmakers JHJ: **Human nucleotide excision repair syndromes: molecular clues to unexpected intricacies.** *Eur J Cancer* 1994, **30A:**1912–1921.
4. Westerveld A, Hoeijmakers JHJ, van Duin M, de Wit J, Odijk H, Pastink A, *et al.*: **Molecular cloning of a human DNA repair gene.** *Nature* 1984, **310:**425–429.
5. van Duin M, Vredeveldt G, Mayne L, Odijk H, Vermeulen W, Klein B, *et al.*: **The cloned human DNA excision repair gene *ERCC-1* fails to correct xeroderma pigmentosum complementation groups A through I.** *Mutat Res* 1989, **217:**83–92.
6. Wood RD: **DNA repair in eukaryotes.** *Annu Rev Biochem* 1996, **65:**135–167.
7. Sijbers AM, de Laat WJ, Ariza RR, Biggerstaff M, Wei Y-F, Moggs JG, *et al.*: **Xeroderma pigmentosum group F caused by a defect in a structure-specific DNA repair endonuclease.** *Cell* 1996, **86:**811–822.
8. Brookman KW, Lamerdin JE, Thelen MP, Hwang M, Reardon JT, Sancar A, *et al.*: ***ERCC4* (*XPF*) encodes a human nucleotide excision repair protein with eukaryotic recombination homologs.** *Mol Cell Biol* 1996, **16:**6553–6562.
9. van Duin M, de Wit J, Odijk H, Westerveld A, Yasui A, Koken MHM, *et al.*: **Molecular characterization of the human excision repair gene *ERCC-1*: cDNA cloning and amino acid homology with the yeast DNA repair gene *RAD10*.** *Cell* 1986, **44:**913–923.
10. Bailly V, Sommers CH, Sung P, Prakash L, Prakash S: **Specific complex formation between proteins encoded by the yeast DNA repair and recombination genes *RAD1* and *Rad10*.** *Proc Natl Acad Sci USA* 1992, **89:**8273–8277.
11. Bardwell L, Cooper AJ, Friedberg EC: **Stable and specific association between the yeast recombination and DNA repair proteins RAD1 and RAD10 *in vitro*.** *Mol Cell Biol* 1992, **12:**3041–3049.
12. Fishman-Lobell J, Haber JE: **Removal of nonhomologous DNA ends in double-strand break recombination: the role of the yeast ultraviolet repair gene *RAD1*.** *Science* 1992, **258:**480–484.
13. Doolittle RF, Johnson MS, Husain I, Houten B, Thomas DC, Sancar A: **Domainal evolution of a prokaryotic DNA repair protein and its relationship to active transport proteins.** *Nature* 1986, **323:**351–353.
14. Sijbers AM, van der Spek PJ, Odijk H, van den Berg J, van Duin M, WesterveldA, *et al.*: **Mutational analysis of the human nucleotide excision repair gene *ERCC1*.** *Nucleic Acids Res* 1996, **24:**3370–3380.
15. McWhir J, Selfridge J, Harrison, DJ, Squires S, Melton DW: **Mice with DNA repair gene (*ERCC-1*) deficiency have elevated levels of p53, liver abnormalities and die before weaning.** *Nat Genet* 1993, **5:**217–224.
16. Thomas KR, Capecchi MR: **Site-directed mutagenesis by gene-targeting in mouse embryo-derived stem cells.** *Cell* 1987, **51:**503–512.
17. van Duin M, van den Tol J, Hoeijmakers JHJ, Bootsma D, Rupp IP, Reynolds P, *et al.*: **Conserved pattern of antisense overlapping transcription in the homologous human *ERCC-1* and yeast *RAD10* DNA repair gene regions.** *Mol Cell Biol* 1989, **9:**1794–1798.
18. Gavrieli Y, Sherman Y, Ben-Sasson SA: **Identification of programmed cell death *in situ via* specific labelling of nuclear DNA fragmentation.** *J Cell Biol* 1992, **119:**493–501.
19. de Vries A, van Oostrom CTM, Hofhuis FMA, Dornant PM, Berg RJW, de Gruijl FR, *et al.*: **Increased susceptibility to ultraviolet-B and carcinogens of mice lacking the DNA excision repair gene *XPA*.** *Nature* 1995, **377:**169–173.
20. Nakane H, Takeuchi S, Yuba S, Saijo M, Nakatsu Y, Murai H, *et al.*: **High incidence of ultraviolet-B- or chemical-carcinogen-induced skin tumours in mice lacking the xeroderma pigmentosum group A gene.** *Nature* 1995, **377:**165–168.
21. Sands AT, Abuin A, Sanchez A, Conti CJ, Bradley A: **High susceptibility to ultraviolet-induced carcinogenesis in mice lacking XPC.** *Nature* 1995, **377:**162–165.
22. Cheo DL, Meira LB, Hammer RE, Burns DK, Doughty ATB, Friedberg EC: **Synergistic interactions between XPC and p53 mutations in double-mutant mice: neural tube abnormalities and accelerated UV radiation-induced skin cancer.** *Curr Biol* 1996, **6:**1691–1694.
23. Johnson JE Jr: **Age-related fine structural changes.** In *Aging and Cell Structure.* Edited by Johnson JE Jr. New York: Plenum Press; 1984, **2:**37–88.
24. Chaudhary AK, Nokubo M, Ramachandra Reddy G, Yeola SN, Morrow JD, Blair IA, *et al.*: **Detection of endogenous malondialdehyde-deoxyguanosine adducts in human liver.** *Science* 1994, **265:**1580–1582.
25. Smith JR, Pereira-Smith OM: **Replicative senescence: implications for *in vivo* aging and tumor suppression.** *Science* 1996, **273:**63–67.
26. Kastan MB, Zhan Q, El-Deiry WS, Carrier F, Jacks T, Walsh WV, *et al.*: **A mammalian cell cycle checkpoint pathway utilizing p53 and GADD45 is defective in ataxia telangiectasia.** *Cell* 1992, **71:**587–597.
27. Cross SM, Sanchez CA, Morgan CA, Schimke MK, Ramel S, Idzerda RL, *et al.*: **A p53-dependent mouse spindle checkpoint.** *Science* 1995, **267:**1353–1365.
28. El-Deiry WS, Tokino T, Velculescu VE, Levy DB, Parsons R, Trent JM, *et al.*: ***WAF1*, a potential mediator of p53 tumor suppression.** *Cell* 1993, **75:**817–825.
29. Wu H, Wade M, Krall L, Grisham J, Xiong Y, van Dyke T: **Targeted *in vivo* expression of the cyclin-dependent kinase inhibitor p21 halts hepatocyte cell-cycle progression, postnatal liver development, and regeneration.** *Genes Dev* 1996, **10:**245–260.
30. Yonish-Rouach E, Resnitzky D, Lotem J, Sachs L, Kimchi A, Oren M: **Wild-type p53 induces apoptosis of myeloid leukaemic cells that is inhibited by interleukin-6.** *Nature* 1991, **352:**345–347.
31. Moriwaki S, Nishigori C, Imamura S, Yagi T, Takahashi C, Fukimoto N, *et al.*: **A case of xeroderma pigmentosum complementation group F with neurological abnormalities.** *Br J Dermatol* 1993, **128:**91–94.
32. Hayakawa H, Ishizaki K, Inoue M, Yagi T, Sekiguchi M, Takebe H: **Repair of ultraviolet radiation damage in xeroderma pigmentosum cells belonging to complementation group F.** *Mutat Res* 1991, **80:**381–388.
33. Burns MA, Tomkins DJ: **Hypersensitivity to mitomycin C cell killing in Roberts syndrome fibroblasts with, but not without, the heterochromatin abnormality.** *Mutat Res* 1989, **216:**243–249.
34. Kunkel TA, Robetts JD, Zakour RA: **Rapid and efficient site-specific mutagenesis without phenotypic selection.** *Methods Enzymol* 1987, **154:**367–382.
35. Sanger F, Nicklen S, Coulson AR: **DNA sequencing with chain-terminating inhibitors.** *Proc Natl Acad Sci USA* 1977, **74:**5463–5467.
36. Smith AG, Hooper M: **Buffalo rat liver cells produce diffusible activity which inhibits the differentiation of murine embryonal carcinoma and embryonic stem cells.** *Dev Biol* 1987, **121:**1–9.
37. Laird PW, Zijderveld A, Linders K, Rudnicki MA, Jaenisch R, Berns A: **Simplified mammalian DNA isolation procedure.** *Nucleic Acids Res* 1991, **19:**4293.
38. Kim DW, Uetsuki T, Kaziro Y, Yamaguchi N, Sugano S: **Use of the human elongation factor 1α promoter as a versatile and efficient expression system.** *Gene* 1990, **91:**217–223.
39. Vermeulen W, Scott RJ, Rodgers S, Müller HJ, Cole J, Arlett CF, *et al.*: **Clinical heterogeneity within xeroderma pigmentosum associated with mutations in the DNA repair and transcription gene *ERCC3*.** *Am J Hum Genet* 1994, **54:**191–200.
40. Simpson RJ, Konijn AM, Lombard M, Raja KB, Salisbury JR, Peters, TJ: **Tissue iron loading and histopathological changes in hypotransferrinaemic mice.** *J Pathol* 1993, **171:**237–244.
41. Di Leonardo A, Linke SP, Clarkin K, Wahl GM: **DNA damage triggers a prolonged p53-dependent G1 arrest and long-term induction of $p21^{Cip1}$ in normal fibroblasts.** *Genes Dev* 1994, **8:**3045–3057.
42. Auffray C, Rougeon F: **Purification of mouse immunoglobin heavy-chain messenger RNAs from myeloma tumor DNA.** *Eur J Biochem* 1980, **107:**303–314.